



Article

Preparation and Characterization of Polyhedron Mn(III) Oxide/ β -Mn(IV) Oxide/Poly-*o*-chloroaniline Porous Nanocomposite for Electroanalytical Photon Detection

Mohamed Rabia ¹, Asmaa M. Elsayed ² and Maha Abdallah Alnuwaiser ^{3,*}

¹ Nanomaterials Science Research Laboratory, Chemistry Department, Faculty of Science, Beni-Suef University, Beni-Suef 62514, Egypt

² TH-PPM Group, Physics Department, Faculty of Science, Beni-Suef University, Beni-Suef 62514, Egypt

³ Department of Chemistry, College of Science, Princess Nourah bint Abdulrahman University, P.O. Box 84428, Riyadh 11671, Saudi Arabia

* Correspondence: maalnuwaiser@pnu.edu.sa

Abstract: Poly-*o*-chloroaniline (POCA) and Mn₂O₃/ β -MnO₂/POCA porous nanocomposite are both synthesized using oxidative polymerization, with K₂S₂O₈ and KMnO₄ as oxidants, respectively. The materials are characterized to confirm their optical, morphological, crystalline, chemical, and elemental properties. The nanocomposite exhibits superior optical properties compared to POCA. The promising optical characteristics make the nanocomposite an attractive candidate for light-sensing applications. Through electrical estimation, the nanocomposite photodetector displays the highest sensitivity between 340 and 440 nm, with J_{ph} (current density) of 0.14 and 0.13 mA cm⁻², correspondingly, and an estimated photon number of 7.4610²¹ and 6.93 × 10²¹ photons/s, respectively. At 340 and 440 nm, the calculated photoresponsivity (R) values are 0.73 and 0.64 mA W⁻¹, respectively, while the estimated detectivity (D) values are 1.64 × 10⁸ and 1.45 × 10⁸ Jones, respectively. These promising results indicate that the fabricated photodetector can soon potentially estimate light wavelengths and photon numbers in various industrial applications.

Keywords: nanocomposite; optoelectronic; Mn₂O₃/ β -MnO₂; poly-*o*-chloroaniline



Citation: Rabia, M.; Elsayed, A.M.; Alnuwaiser, M.A. Preparation and Characterization of Polyhedron Mn(III) Oxide/ β -Mn(IV) Oxide/Poly-*o*-chloroaniline Porous Nanocomposite for Electroanalytical Photon Detection. *Processes* **2023**, *11*, 2375. <https://doi.org/10.3390/pr11082375>

Academic Editors: Wanjun Wang and Zhuofeng Hu

Received: 14 June 2023

Revised: 26 July 2023

Accepted: 26 July 2023

Published: 7 August 2023



Copyright: © 2023 by the authors. Licensee MDPI, Basel, Switzerland. This article is an open access article distributed under the terms and conditions of the Creative Commons Attribution (CC BY) license (<https://creativecommons.org/licenses/by/4.0/>).

1. Introduction

Devices that are used to detect images have the ability to generate an electrical signal under the illumination process. These devices are now widely used in our societies, in many industries such as the automotive industry, through medical, biological, and even military applications. These developed devices achieve outstanding performance using these materials with low dimensions [1,2]. The principle used for the photodetector is to work under light intensity or different wavelengths, which are produced by activating the surface of the photodetector with light radiation, to produce a hot free electron; this produces current values [3–5]. Light is detected for these materials by allowing photons to stream through their active sites. Increasing the active sites has become the interest of researchers. Therefore, nanomaterials have been produced by synthesizing active sites, increasing surface area, and manufacturing them in different geometric shapes.

In general, broadband semiconductors composed of metal oxide or polymers have material-friendly properties and excellent environmental sustainability [6]. This dependence on metal oxide is related to the great stability and the optical response in wide spectra.

By basic criteria for UV detectors or solar blinds, narrow-range sensitivity and high processing cost would limit their practical applications. Recently, Li et al. [7] reported solar photodetector based on the heterocore Ga₂O₃/CuSCN, which gives a weak response related to the small produced J_{ph} value (24 × 10⁻¹⁵ mA) at 2.0 V. Moreover, various materials such as sulfides and carbon derivatives can be applied in these applications [8,9].

Scientists and researchers are actively working on developing conducting polymers with optical applications to be utilized in advanced devices like solar cells and optoelectronics. These materials possess unique properties such as long chains and high compactness, coupled with the added advantage of conductivity. The combination of these features makes them highly desirable for integration into cutting-edge technological devices.

One of the key advantages of using conducting polymers is their cost-effectiveness. These materials can be produced at a relatively low cost compared to traditional inorganic semiconductors. Additionally, their high correlation rate with the desired optical and electrical properties enhances their applicability in various devices.

However, a significant challenge lies in ensuring that the efficiency of these materials matches the requirements of the new technology employed in these devices. The conducting polymers need to demonstrate high performance and compatibility with the specific demands of solar cells and optoelectronics. Researchers are working towards optimizing the synthesis methods and material properties to achieve the desired efficiency levels, while also addressing issues such as stability, scalability, and long-term performance.

By overcoming these challenges and further improving the efficiency of conducting polymers, scientists aim to enhance the capabilities of highly sensitive devices, ultimately leading to advancements in renewable energy generation, efficient lighting, and other optical applications.

Metal oxide with polymer composite has additional light-sensing properties that are suitable for commercial photodetectors, designed due to their high mobility and efficient responses, which are better than ohmic contact photodetectors, and conductive photodetectors are preferred for their fast response [10,11]. But there is a trade-off between device response and response speed under the influence of surface defects and carrier drift dynamics [12–14].

Aniline and its derivatives, including o-chloroaniline, benzodithiophene/fluorine, or triphenylamine, have demonstrated excellent response to light radiation when applied intraretinally [15], in addition to their electrical behavior [16,17]. Theoretical studies of aniline derivatives have shown that the resulting compounds possess favorable optical properties and respond well to light. Experimental studies have also confirmed this behavior with a measured J_{ph} of 0.001 mA.

To enhance the optoelectronic properties of aniline-based materials, scientists employ various strategies. One approach is to prepare the polymer with highly desirable morphological properties that facilitate efficient light absorption. By controlling the structure and organization of the polymer chains, researchers can optimize the material's ability to absorb light. Another method involves coating the polymer with additional metal oxide materials that possess it. This composite structure combines the unique properties of the aniline polymer with the enhanced light absorption capabilities of the metal oxide. The coating helps to overcome the limitations of pure polymers and improves their overall optical behavior.

Moreover, scientists aim to utilize these cost-effective materials in highly technological devices while achieving comparable efficiency to that of inorganic materials. In some cases, these polymer composites can even surpass the performance of novel materials like graphene or silicon. The advantage of aniline-based materials lies in their low-cost production, ease of processing, and tunability of their properties. By optimizing their optical behavior and tailoring their structure, scientists can harness the benefits of these materials for a wide range of optoelectronic applications, such as sensors and photodetectors. This research contributes to the ongoing advancement of cost-effective and efficient materials for high-tech devices [18].

By achieving a very fine thin film behavior in polymer composites, scientists can unlock additional advantages that have the potential to surpass the properties of existing materials. When the polymer composite is confined to a fine structure, such as a thin film or layered arrangement, it exhibits unique properties that can overcome the limitations of conventional materials.

This behavior of the polymer composite provides enhanced control over its electronic and optical properties. This leads to improved charge transport, increased mobility, and efficient light absorption and emission. The superior control and performance offered by this fine particle behavior can surpass the capabilities of recent materials like graphene and silicon.

Furthermore, the nature of the polymer composite results in desirable characteristics such as mechanical flexibility, transparency, and tunability. These properties make it suitable for various applications including flexible electronics, wearable devices, and transparent displays, in which the polymer composite adds to its potential for overcoming the limitations of current materials.

Scientists and researchers are actively working to harness the advantages of thin film behavior to develop advanced materials that outperform existing ones in terms of performance, cost-effectiveness, and versatility. Ongoing advancements in this field have the potential to revolutionize various technological industries and pave the way for innovative applications in the future [19–21].

In this study, POCA and $\text{Mn}_2\text{O}_3/\beta\text{-MnO}_2/\text{POCA}$ nanocomposite thin film is synthesized using oxidative polymerization with $\text{K}_2\text{S}_2\text{O}_8$ and KMnO_4 as oxidants. The nanocomposite shows high optical properties for light sensing by monitoring the wavelengths through the optical absorption curve. Electroanalytical estimation is used to determine the photon numbers by testing the nanocomposite photodetector under various wavelengths till 730 nm. The R, linear dynamic range (LDR), and D values are also determined for the photodetector, which suggests its potential application in a wide range of optical technological devices in the near future. The $\text{Mn}_2\text{O}_3/\beta\text{-MnO}_2/\text{POCA}$ nanocomposite photodetector demonstrates its ability to accurately quantify the number of photons by measuring the photo-generated electrons under various monochromatic lights. This measurement is achieved with minimal noise, as evidenced by the low values of J_0/J_{ph} percentage, further validating its reliable performance in photon detection.

2. Experimental Section

2.1. Materials

O-chloroaniline (99.2%) was obtained from Merck, Germany. Pio-Chem Co. (Giza, Egypt) supported us with $\text{K}_2\text{S}_2\text{O}_8$ (99.5%). Moreover, El-Nasr company (Cairo, Egypt) supported us with KMnO_4 (99.8%). HCl (36%) was obtained from Winlab Co., Watford, UK.

2.2. $\text{Mn}_2\text{O}_3/\beta\text{-MnO}_2/\text{POCA}$ Nanocomposite Preparation

The $\text{Mn}_2\text{O}_3/\beta\text{-MnO}_2/\text{POCA}$ nanocomposite is prepared through the polymerization of o-chloroaniline by KMnO_4 as both an oxidizing and doping agent. The oxidation reaction enables the incorporation of Mn compounds into the polymer with oxidation state of Mn (III) or Mn (IV). The process is carried out in a 0.7 M HCl solution that serves as both a solvent and an acid medium. The resulting precipitate, which is brownish-green in color, is then collected and subjected to further treatment; Figure 1.

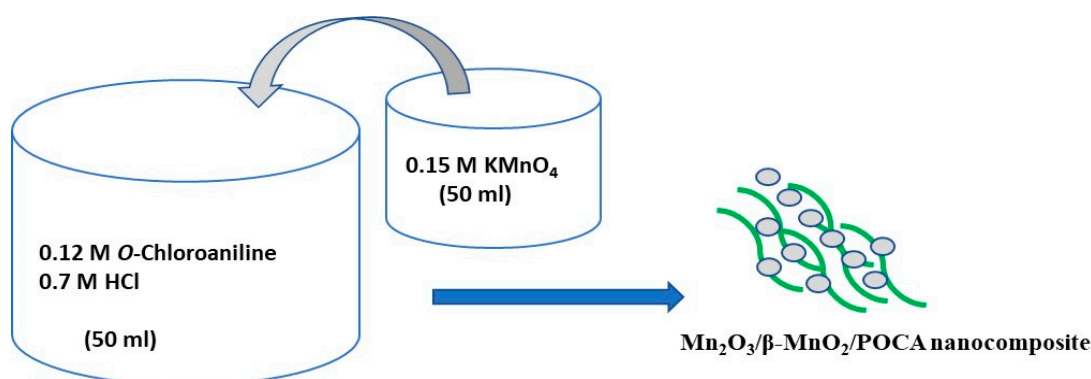


Figure 1. Schematic diagram of the preparation of $\text{Mn}_2\text{O}_3/\beta\text{-MnO}_2/\text{POCA}$ nanocomposite.

2.3. Characterization Tools

The elemental and compositional analysis of the nanocomposite is performed using various characterization techniques, including FTIR, XPS, and XRD, using instruments such as Jasco model 340, Kratos Analytical, Manchester, UK; and PANalytical Pro. Additionally, the topography and morphological properties of the materials are estimated using SEM and TEM, which are carried out using ZEISS and JEOL instruments, respectively.

2.4. The Electroanalytical Measurements

The electroanalytical study involves the use of the $\text{Mn}_2\text{O}_3/\beta\text{-MnO}_2/\text{POCA}$ film to estimate the number of photons using a photodetector. The film is covered on one side with Ag paste. The optical response of the photodetector enables it to sense light and estimate the number of photons under various wavelengths: 340–730 nm. The CHI608E is used to perform this electrical study under a halide lamp. The study enables the calculation of the R and D efficiency behavior of the photodetector.

3. Results and Discussion

3.1. Analyses

Based on the XRD pattern presented in Figure 2a, the elemental and chemical composition of the prepared $\text{Mn}_2\text{O}_3/\beta\text{-MnO}_2/\text{POCA}$ sample can be inferred. The crystalline peaks observed at 32.3° , 34.17° , and 35.9° indicate the presence of Mn_2O_3 in the sample. These peaks correspond to the (310), (222), and (123) growth directions of Mn_2O_3 , respectively [22].

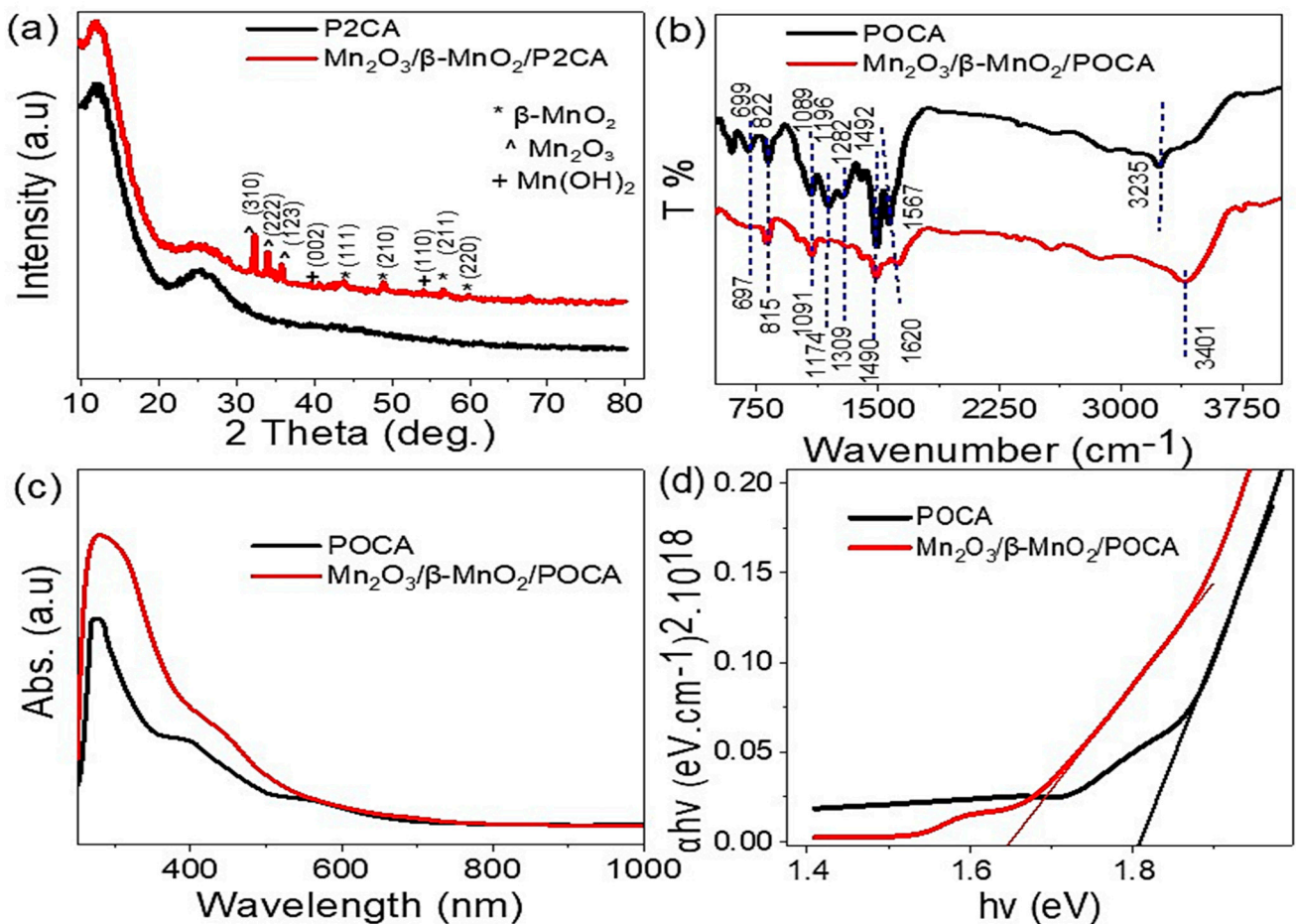


Figure 2. (a–d) shows XRD pattern, FTIR spectroscopy, optical behavior, and bandgap of $\text{Mn}_2\text{O}_3/\beta\text{-MnO}_2/\text{POCA}$ nanocomposite, correspondingly.

Additionally, the XRD pattern shows the presence of β -MnO₂ in the sample, as evidenced by the crystalline peaks observed at 43.9°, 49.2°, 56.6°, and 59.6°. These peaks correspond to the (111), (210), (211), and (220) growth directions of β -MnO₂ and are consistent with the JCPDS 24-0735 reference [22].

The POCA material of the sample is not directly detected by XRD analysis, as it does not produce characteristic peaks in the XRD pattern.

In addition to the Mn₂O₃ and β -MnO₂ peaks, the XRD pattern also shows two peaks at 39.6° and 54.1°, which can be attributed to Mn(OH)₂ in the sample. These peaks correspond to the (002) and (110) growth directions of Mn(OH)₂, correspondingly.

Regarding the POCA material, the XRD pattern indicates a broad peak, which is characteristic of an amorphous structure. After the formation of the Mn₂O₃/ β -MnO₂/POCA composite, there is no enhancement in the crystalline structure of POCA, indicating that it remains in an amorphous state. This is a common occurrence in many polymeric materials [19]. However, its presence can be inferred from other analysis techniques, such as FTIR spectroscopy.

It should be noted that in this composite, the POCA component is primarily used as a container for the Mn oxides and does not contribute significantly to the crystalline structure of the composite.

The black curve in Figure 2b describes the chemical structure of POCA, which has been verified through FTIR analyses. The band at 3225 cm⁻¹ matches the N-H group in the polymer. The two bands at 1567 and 1492 cm⁻¹ match the C-C and C=C structure, respectively [17]. The C-N vibration group is identified through the band at 1282 cm⁻¹, while the out-of-plan C-H group is represented by two bands at 1089 and 822 cm⁻¹. Finally, the insertion of Cl⁻ through the N-H group is confirmed through the band at 699 cm⁻¹.

The red curve in Figure 2b demonstrates the FTIR of the Mn₂O₃/ β -MnO₂/POCA nanocomposite, which exhibits the same bands as the POCA polymer, but with additional shifts towards the red side in most of the bands. This shift is an indication that the composite has formed and that Mn₂O₃/ β -MnO₂ has attached to the polymer materials [19]. Additionally, there is a greater intensity in the band at 3401 cm⁻¹, which is evidence of the formation of OH⁻ groups within the composite.

The optical characteristics of POCA and Mn₂O₃/ β -MnO₂/POCA are illustrated in Figure 2c,d, correspondingly. The absorption spectra of both the polymer and the composite exhibit strong absorbance in the UV and Vis spectra ranging from 250 to 630 nm. Although POCA displays a wide absorption band, the incorporation of Mn₂O₃/ β -MnO₂ enhances the absorbance intensity in these regions, resulting in a composite with greater optical absorbance. This observation is further confirmed by the bandgap analysis, with the Mn₂O₃/ β -MnO₂/POCA composite displaying a promising bandgap of 1.65 eV. The bandgap is determined using Equations (1) and (2), where Equation (1) involves α , which is calculated using the absorbance (A) and the material density (d). Equation (2) incorporates additional constants such as the Planck constant (h) and the frequency (ν).

$$\alpha = \left(\frac{2,303}{d} \right) A \quad (1)$$

$$\alpha h\nu = A(h\nu - E_g)^{1/2} \quad (2)$$

SEM images of POCA and the Mn₂O₃/ β -MnO₂/POCA nanocomposite, shown in Figure 3a,b, respectively, reveal significant differences in morphology before and after the composite formation. The POCA polymer appears fibrous, while the Mn₂O₃/ β -MnO₂/POCA nanocomposite has a porous structure and a polyhedral shape with an average length of 150 nm; this reflects the effect of insertion of Mn₂O₃/ β -MnO₂ into the polymer matrix to enhance the polyhedron's behavior.

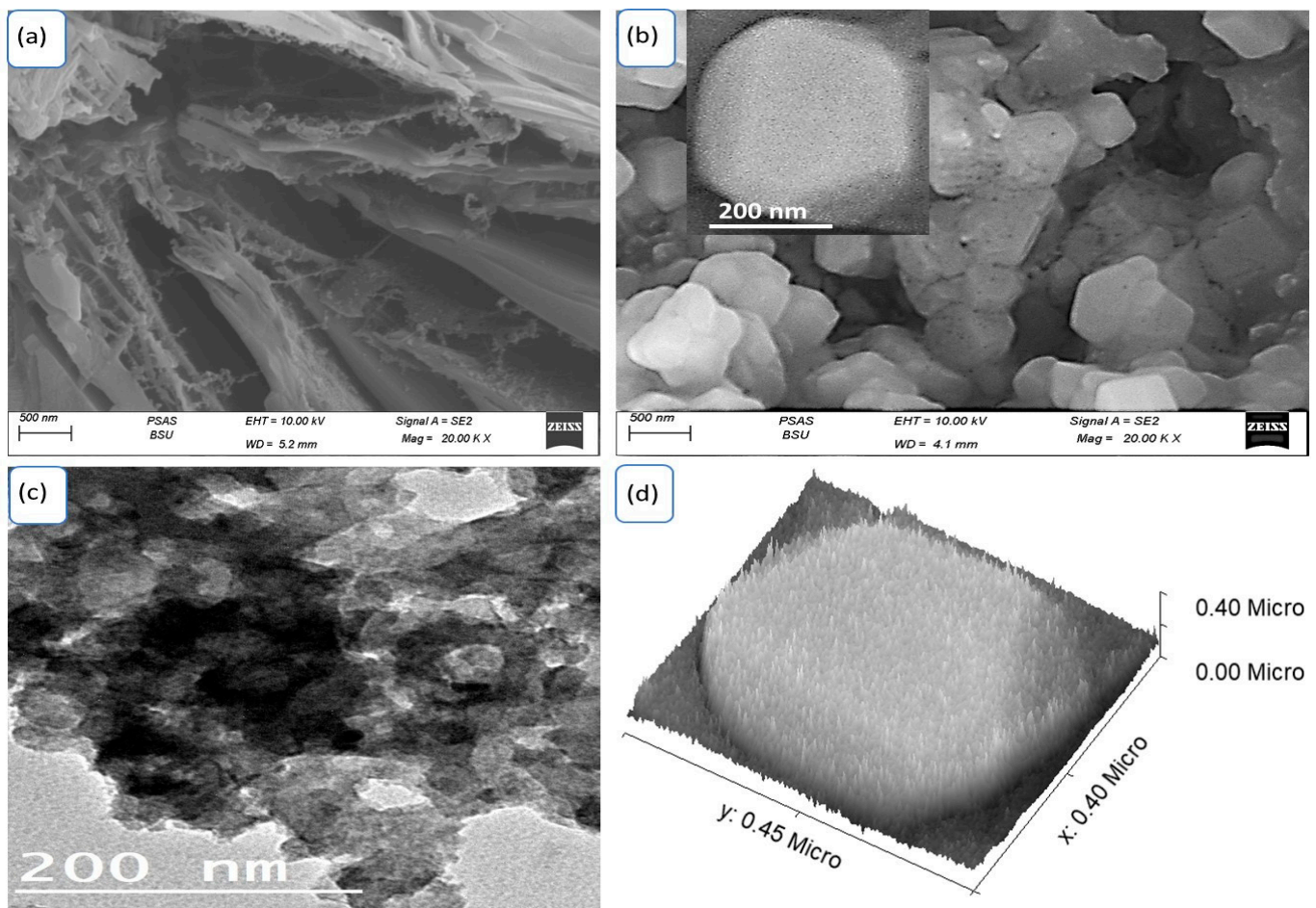


Figure 3. (a) SEM of POCA. SEM (b), TEM (c), and (d) theoretical simulated of $\text{Mn}_2\text{O}_3/\beta\text{-MnO}_2/\text{POCA}$ nanocomposite.

The TEM image in Figure 3c shows that the $\text{Mn}_2\text{O}_3/\beta\text{-MnO}_2/\text{POCA}$ nanocomposite has a porous and polyhedral structure, where the dark color represents the $\text{Mn}_2\text{O}_3/\beta\text{-MnO}_2$ particles that have penetrated into the grey-colored POCA. Additionally, Figure 3d confirms the polyhedral structure of the $\text{Mn}_2\text{O}_3/\beta\text{-MnO}_2/\text{POCA}$ composite using the Gwydion program to simulate material roughness. The simulation was based on a particle size of $0.4 \times 0.45 \mu\text{m}$, which clearly shows the polyhedron structure.

The XPS data (Figure 4a–f) reveal the valency state and elemental composition of the $\text{Mn}_2\text{O}_3/\beta\text{-MnO}_2/\text{POCA}$ nanocomposite. The survey in Figure 4a shows the presence of N, O, Cl, C, and Mn elements with high accuracy. Figure 4b indicates a dual-oxidation state of Mn (+3 and +2) for Mn $2\text{P}_{3/2}$ and $2\text{P}_{1/2}$ at 643 and 654 eV, correspondingly, with an energy gap of 11 eV. The O 1s in Figure 4c appears at 533.1 eV, related to chemical bonds with Mn oxides. The C elements at 286 eV in Figure 4d relate to C=C, C-N, C-Cl, and C-C groups inside the POCA, while Figure 4e shows N 1s at 401 eV related to N in the POCA, and Figure 4f reveals Cl 1p at 201 eV for the same polymer compound. The XPS position of these elements confirms the formation and chemical connections of $\text{Mn}_2\text{O}_3/\beta\text{-MnO}_2$ inside the POCA composite.

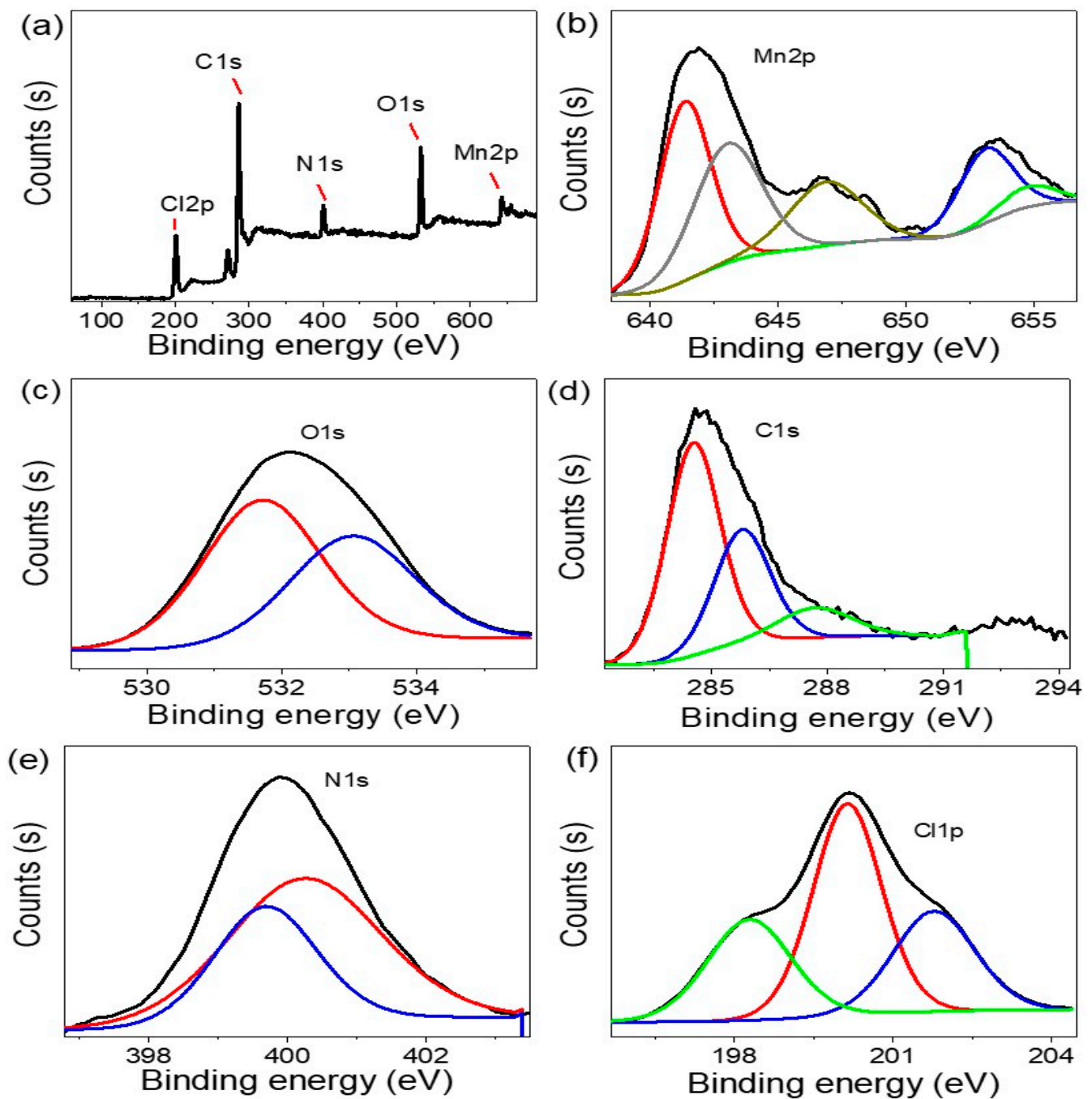


Figure 4. The XPS spectra (0.83 nm) of (a) $\text{Mn}_2\text{O}_3/\beta\text{-MnO}_2/\text{POCA}$ survey, (b) Mn, (c) O, (d) C, (e) N, and (f) Cl elements spectra.

3.2. Electrical Study

The sensitivity of the $\text{Mn}_2\text{O}_3/\beta\text{-MnO}_2/\text{POCA}$ nanocomposite photodetector to light radiation was evaluated by measuring its electrical properties using a CHI608E instrument in applied bias voltage from -2.0 to $+2.0$ V. When the nanocomposite film was exposed to light radiation, the semiconductor Mn oxides with the POCA absorbed the photons and split the external energy levels, resulting in a bandgap of 1.65 eV. This bandgap is smaller than the energy of photons in the visible region (1.95–3.26 eV), which means that the energy from the light is sufficient to split the levels and transfer electrons to the outer levels. This process occurs in two steps: the first is the generation of photocarriers, and the second is the transfer of these carriers to the outer level to produce hot electrons. The density of

these hot electrons can be represented by the J_{ph} value produced by the device. Figure 5 shows the J_{ph} value and the dark current (J_o , black curve) of the nanocomposite film. The J_{ph} value represents the photocurrent that is greater than J_o , and its value is 0.15 mA/cm^2 , while the dark current is $3.0 \text{ } \mu\text{A/cm}^2$. The lamp used for the measurements has an intensity of 100 mW/cm^2 , and the photon number is $8.0 \times 10^{21} \text{ photons/s}$, using Equation (3). The J_{ph} value of 0.15 mA/cm^2 was generated by this number of photons, as shown in Figure 6.

$$N\lambda P/hc \quad (3)$$

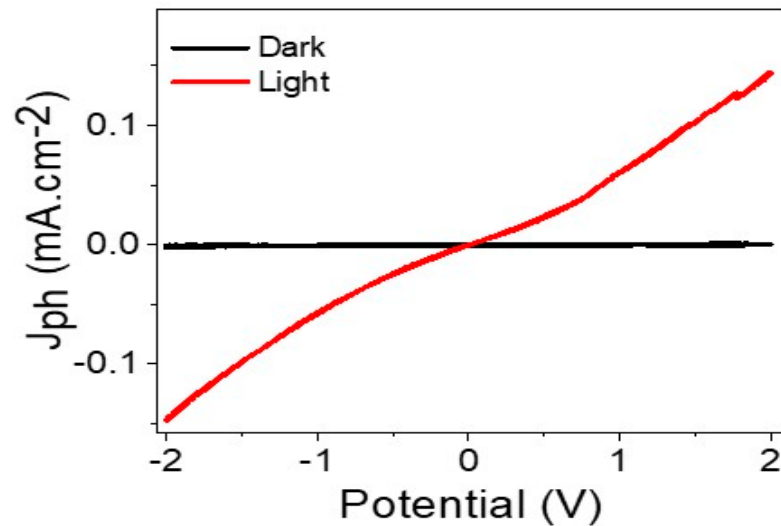


Figure 5. The electrical behavior of $\text{Mn}_2\text{O}_3/\beta\text{-MnO}_2/\text{POCA}$ nanocomposite photodetector through the photocurrent (J_{ph}) and dark current (J_o) generation.

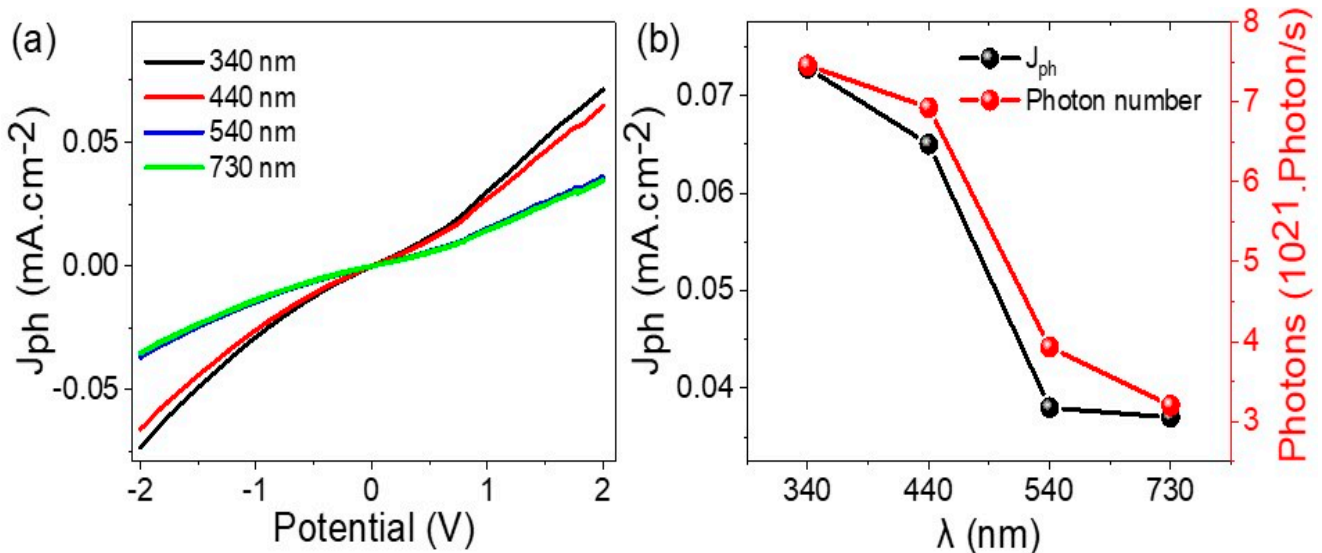


Figure 6. (a) The response of $\text{Mn}_2\text{O}_3/\beta\text{-MnO}_2/\text{POCA}$ nanocomposite photodetector and (b) the produced photogenerated J_{ph} equivalent to the used photons under various monochromatic lights (340–730 nm).

The sensitivity of the $\text{Mn}_2\text{O}_3/\beta\text{-MnO}_2/\text{POCA}$ nanocomposite photodetector can be determined by measuring its response to various monochromatic lights. Figure 6a shows that the photodetector has different levels of photocurrent production depending on the incidence wavelengths, indicating its varying sensitivity across the optical region. The highest sensitivity is observed between 340 and 440 nm, with J_{ph} values of 0.14 and 0.13 mA cm^{-2} , correspondingly. According to Equation (3), the estimated photon number

is 7.46×10^{21} and 6.93×10^{21} photon/s, respectively. The photodetector also produces a decent photocurrent in the mid-visible (540 nm) or IR (730 nm) regions, with J_{ph} values of 0.07 and 0.06 mA cm⁻², respectively. This suggests that the number of produced photons is 3.96×10^{21} and 3.20×10^{21} photon/s, respectively. Figure 6b depicts the relationship between various wavelengths, and the produced J_{ph} indicates the estimated photon number associated with these wavelengths. This confirms that the Mn₂O₃/β-MnO₂/POCA nanocomposite photodetector can electroanalytically estimate the number of photons through the photogenerated electrons produced under various monochromatic lights.

The Mn₂O₃/β-MnO₂/POCA nanocomposite photodetector efficiency evaluated under consideration exhibits favorable values for the evaluation of the three key parameters: D, LDR, and R. These characteristics, combined with low noise levels, indicate that the photodetector holds great promise for electroanalytical photon sensing across a wide range of high-tech applications. The R value is a crucial factor that measures the ability of this optical device to convert light into an electrical signal. The higher the responsivity value, the more efficient the device is at converting photons into usable electrical current. The promising values of responsivity in the photodetector indicate that it can effectively capture and convert light signals, making it suitable for photon sensing applications. The LDR signifies the sensitivity of the photodetector in distinguishing between light and dark conditions. A high LDR indicates that the device has a significant change in electrical resistance when exposed to light, enabling it to discern even small variations in light intensity. The favorable LDR value suggests that the photodetector can detect subtle changes in light levels, making it well-suited for precise photon sensing.

The D value combines responsivity, noise, and bandwidth considerations to provide an overall measure of the photodetector's sensitivity. A higher detectivity value indicates improved sensitivity in detecting weak light signals against a background noise level. The promising detectivity value of the photodetector highlights its ability to detect even low-intensity light signals accurately and reliably.

In addition to the parameters, the low noise exhibited by the photodetector is another positive aspect. Low noise levels imply that the device produces minimal unwanted electrical signals or disturbances, allowing for accurate and reliable detection of light signals. This characteristic is crucial for precise measurements and sensing applications.

The photoresponsivity of the Mn₂O₃/β-MnO₂/POCA nanocomposite photodetector is evaluated by calculating the R value (photocurrent to incident power density). The surface area of the photodetector is denoted by S, as shown in Figure 7a. The R values exhibit the same trend as the photocurrent and the generated hot electrons, with the highest values observed at 340 and 440 nm, where R equals 0.73 and 0.64 mA W⁻¹, respectively. The R values decrease to 0.38 and 0.37 mA W⁻¹ at 540 and 730 nm, respectively. Despite the decrease in the R values in the mid-vis and IR regions, the values are still significant, indicating the photoresponsivity of the Mn₂O₃/β-MnO₂/POCA nanocomposite photodetector in these regions. This result confirms the broad optical sensitivity of the photodetector.

$$R = \frac{J_{ph} - J_d}{P.S} \quad (4)$$

The linear dynamic range (LDR) [23,24] of the Mn₂O₃/β-MnO₂/POCA nanocomposite photodetector can be calculated using Equation (5). The LDR at 340 nm was evaluated to be 77, indicating a high sensitivity of the photodetector for detecting photons.

$$LDR = 20 \cdot \log \left(\frac{J_{ph}}{J_o} \right) \quad (5)$$

$$D = R \sqrt{S / 2 e J_o} \quad (6)$$

$$\text{Noise radiation} = J_o / J_{ph} \quad (7)$$

The sensitivity of the $\text{Mn}_2\text{O}_3/\beta\text{-MnO}_2/\text{POCA}$ nanocomposite photodetector can be quantified by the D value, which is related to the R value. The D value, which represents the photodetector efficiency to the light radiation, can be estimated using the electron charge (e) and the generated electrons on the photodetector surface. The D values for the photodetector under a range of monochromatic lights are shown in Figure 7b and calculated using Equation (6) [25,26]. At wavelengths of 340 and 440 nm, the D values are 1.64×10^8 and 1.45×10^8 Jones, respectively. The low values of noise, represented as the percentage of J_0/J_{ph} , suggest that the photodetector has negligible noise. The good values of R , LDR, and D , along with the low noise, indicate that this photodetector has promising potential for electroanalytical photon sensing in various high-tech applications.

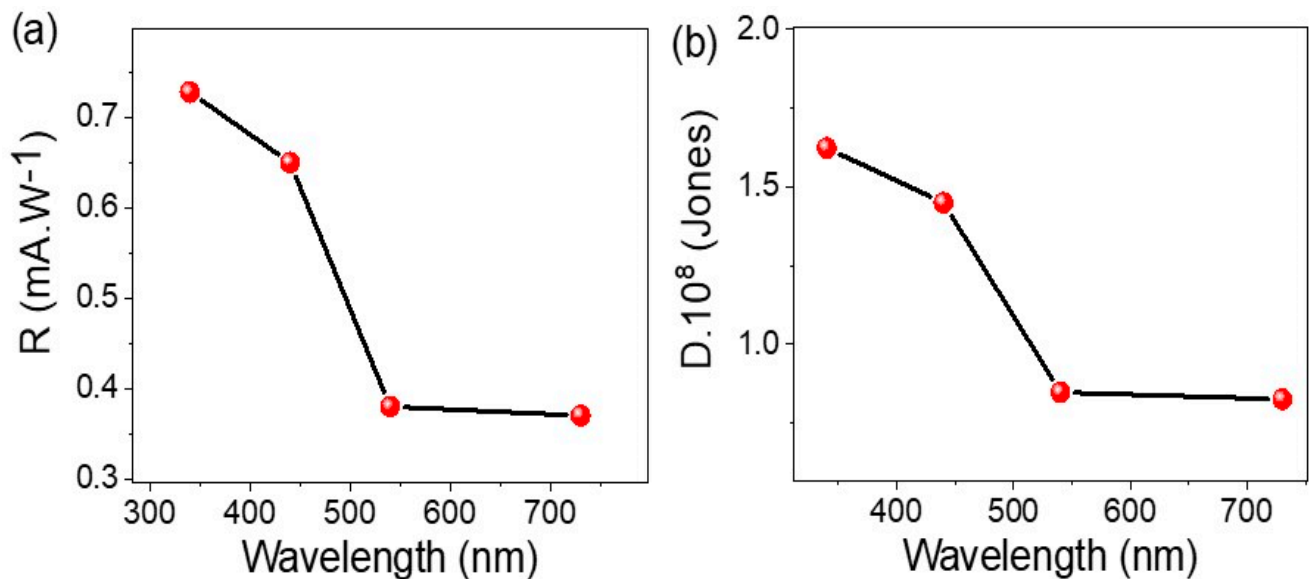


Figure 7. The efficiency of the fabricated $\text{Mn}_2\text{O}_3/\beta\text{-MnO}_2/\text{POCA}$ nanocomposite photodetector through estimation of (a) R and (b) D values.

Collectively, the favorable values of responsivity, light-to-dark resistance ratio, detectivity, and low noise in the photodetector indicate its promising potential for electroanalytical photon sensing in various high-tech applications. These applications may include areas such as biomedical diagnostics, environmental monitoring, telecommunications, and optical data communications, where reliable and sensitive detection of light signals is crucial. With its impressive performance parameters, this photodetector offers a valuable tool for advancing photon-sensing technologies and contributing to advancements in high-tech industries.

Table 1 confirms the superiority of the produced value for the $\text{Mn}_2\text{O}_3/\beta\text{-MnO}_2/\text{POCA}$ nanocomposite photodetector compared to the other previous studies. Based on Equation (7), the noise is related to the ratio of J_0 (dark current) to J_{ph} (photocurrent). When the value of J_0 is negligible, such as in the case of $3 \mu\text{A}$, the noise is calculated to be 1.5%. This indicates that the noise contribution is limited and relatively ineffective.

Table 1. The efficiency of the fabricated $\text{Mn}_2\text{O}_3/\beta\text{-MnO}_2/\text{POCA}$ nanocomposite photodetector through estimation of R in compared to the other work.

Electrode	λ (nm)	Bais (V)	R (mAW^{-1})
CuO/Si Nanowire [27]	405	0.2	3.8×10^{-3}
Graphene/GaN [28]	365	7	3×10^{-3}
TiO ₂ -PANI [29]	320	0	3×10^{-3}
GO/Cu ₂ O [30]	300	2	0.5×10^{-3}

Table 1. Cont.

Electrode	λ (nm)	Bais (V)	R (mAW ⁻¹)
Graphene/P3HT [31]	325	1	NA
ZnO/Cu ₂ O [32]	350	2	4×10^{-3}
ZnO-CuO [33]	405	1	3×10^{-3}
PbI ₂ -graphene [34]	550	2	NA
PbI ₂ -5%Ag [35]	532	6	NA
CuO nanowires [36]	390	5	-
TiN/TiO ₂ [37]	550	5	-
ZnO /RGO [38]	350	5	1.3×10^{-3}
Se/TiO ₂ [39]	450	1	5×10^{-3}
ZnO /RGO [38]	350	5	1.3×10^{-3}
Mn ₂ O ₃ /β-MnO ₂ /POCA (this work)	440	2	0.73

4. Conclusions

A polyhedron-shaped Mn₂O₃/β-MnO₂/POCA nanocomposite with excellent morphological and optical properties has been synthesized through doping polymerization. This nanocomposite exhibits a high absorption value, which is indicative of a good bandgap of 1.65 eV. Due to these optical and morphological properties, the nanocomposite can detect light in a broad optical range. The highest sensitivity is observed between 340 and 440 nm, with J_{ph} values of 0.14 and 0.13 mA cm⁻², respectively, and estimated photon numbers of 7.46×10^{21} and 6.93×10^{21} photons/s, correspondingly. At 340 and 440 nm, the calculated R values are 0.73 and 0.64 mA W⁻¹, respectively, while the estimated D values are 1.64×10^8 and 1.45×10^8 Jones, respectively. This demonstrates that the Mn₂O₃/β-MnO₂/POCA nanocomposite photodetector is capable of electrochemically quantifying the number of photons by measuring the photogenerated electrons generated under different monochromatic lights, under the estimated minimal (negligible) noise, as indicated by the low values of J_o/J_{ph} percentage. This promising behavior suggests that the fabricated photodetector has potential applications in estimating light wavelengths and photon numbers in various industrial settings in the near future.

Author Contributions: The authors shared equally in writing, revision, and supervision. Experiments were performed by M.R. and A.M.E. Funding acquisition: M.A.A. All authors have read and agreed to the published version of the manuscript.

Funding: Princess Nourah bint Abdulrahman University Researchers Supporting Project number (PNURSP2023R186), Princess Nourah bint Abdulrahman University, Riyadh, Saudi Arabia.

Data Availability Statement: All data generated or analyzed during this study are included in this article.

Acknowledgments: Princess Nourah bint Abdulrahman University Researchers Supporting Project number (PNURSP2023R186), Princess Nourah bint Abdulrahman University, Riyadh, Saudi Arabia.

Conflicts of Interest: The authors have no conflict of interest.

References

- Huang, H.Y.; Chen, J.H.; Nan, F.; Lin, Y.; Zhou, L. Enhancement of near Ultraviolet Spectral Range Responsibility of Silicon Photodetectors via Additional Fluorescent InP/ZnS Quantum Dots Layer. *Opt. Laser Technol.* **2023**, *166*, 109608. [CrossRef]
- Chao, J.; Zhang, K.; Meng, D. Simple-Grown SnO₂ Microflowers/Carbon Cloth as Rigid and Flexible Ultraviolet Photodetectors. *Mater. Lett.* **2023**, *350*, 134912. [CrossRef]
- Wang, J.; Chen, J. Ag Nanoparticles Enhanced PbS QDs/Graphene/Si near-Infrared Photodetector. *Phys. E Low-Dimens. Syst. Nanostruct.* **2023**, *154*, 115793. [CrossRef]

4. Zhao, J.; Liu, H.; Deng, L.; Du, Y.; Wang, J.; Wen, S.; Wang, S.; Zhu, Z.; Xie, F.; Liu, W. Photovoltaic High-Performance Broadband Photodetector Based on the Heterojunction of MoS₂/Silicon Nanopillar Arrays. *Appl. Surf. Sci.* **2023**, *638*, 157994. [[CrossRef](#)]
5. Deng, S.; Guo, H.; Yan, J.; Zhu, D.; Li, J.; Qiao, M.; Xie, J. NIR-UV Dual-Mode Photodetector with the Assistance of Machine-Learning Fabricated by Hybrid Laser Processing. *Chem. Eng. J.* **2023**, *472*, 144908. [[CrossRef](#)]
6. Sreedhar, A.; Ta, Q.T.H.; Noh, J.-S. Versatile Role of 2D Ti₃C₂ MXenes for Advancements in the Photodetector Performance: A Review. *J. Ind. Eng. Chem.* **2023**. [[CrossRef](#)]
7. Li, S.; Guo, D.; Li, P.; Wang, X.; Wang, Y.; Yan, Z.; Liu, Z.; Zhi, Y.; Huang, Y.; Wu, Z.; et al. Ultrasensitive, Superhigh Signal-to-Noise Ratio, Self-Powered Solar-Blind Photodetector Based on n-Ga₂O₃/p-CuSCN Core-Shell Microwire Heterojunction. *ACS Appl. Mater. Interfaces* **2019**, *11*, 35105–35114. [[CrossRef](#)]
8. Shaban, M.; Abukhadra, M.R.; Rabia, M.; Elkader, Y.A.; Abd El-Halim, M.R. Investigation the Adsorption Properties of Graphene Oxide and Polyaniline Nano/Micro Structures for Efficient Removal of Toxic Cr(VI) Contaminants from Aqueous Solutions; Kinetic and Equilibrium Studies. *Rend. Lincei* **2018**, *29*, 141–154. [[CrossRef](#)]
9. Abukhadra, M.R.; Rabia, M.; Shaban, M.; Verpoort, F. Heulandite/Polyaniline Hybrid Composite for Efficient Removal of Acidic Dye from Water; Kinetic, Equilibrium Studies and Statistical Optimization. *Adv. Powder Technol.* **2018**, *29*, 2501–2511. [[CrossRef](#)]
10. Shaikh, N.S.; Ubale, S.B.; Mane, V.J.; Shaikh, J.S.; Lokhande, V.C.; Praserthdam, S.; Lokhande, C.D.; Kanjanaboos, P. Novel Electrodes for Supercapacitor: Conducting Polymers, Metal Oxides, Chalcogenides, Carbides, Nitrides, MXenes, and Their Composites with Graphene. *J. Alloys Compd.* **2022**, *893*, 161998. [[CrossRef](#)]
11. Xu, Z.; Chu, X.; Wang, Y.; Zhang, H.; Yang, W. Three-Dimensional Polymer Networks for Solid-State Electrochemical Energy Storage. *Chem. Eng. J.* **2020**, *391*, 123548. [[CrossRef](#)]
12. Yu, X.; Marks, T.J.; Facchetti, A. Metal Oxides for Optoelectronic Applications. *Nat. Mater.* **2016**, *15*, 383–396. [[CrossRef](#)]
13. Elsayed, A.M.; Rabia, M.; Shaban, M.; Aly, A.H.; Ahmed, A.M. Preparation of Hexagonal Nanoporous Al₂O₃/TiO₂/TiN as a Novel Photodetector with High Efficiency. *Sci. Rep.* **2021**, *11*, 17572. [[CrossRef](#)]
14. Zhang, M.; Xiong, Z.; Jia, J.; Zhou, Z.; Wu, B.; Ni, Y.; Zhou, X.; Cao, L. Improving Electrochemical Performance of Hollow Cr₂O₃/CrN Nanoshells as Electrode Materials for Supercapacitors. *J. Electroanal. Chem.* **2020**, *856*, 113696. [[CrossRef](#)]
15. Liu, Y.; Guo, P.; Gao, P.; Tong, J.; Li, J.; Wang, E.; Wang, C.; Xia, Y. Effect of Fluorine Atoms on Optoelectronic, Aggregation and Dielectric Constants of 2,1,3-Benzothiadiazole-Based Alternating Conjugated Polymers. *Dye. Pigment.* **2021**, *193*, 109486. [[CrossRef](#)]
16. Ahmad, M.N.; Rafique, F.; Nawaz, F.; Farooq, T.; Anjum, M.N.; Hussain, T.; Hassan, S.; Batool, M.; Khalid, H.; Shehzad, K. Synthesis of Antibacterial Poly(o-Chloroaniline)/Chromium Hybrid Composites with Enhanced Electrical Conductivity. *Chem. Cent. J.* **2018**, *12*, 46. [[CrossRef](#)]
17. Linganathan, P.; Sundararajan, J.; Samuel, J.M. Synthesis, Characterization, and Photoconductivity Studies on Poly(2-Chloroaniline) and Poly(2-Chloroaniline)/CuO Nanocomposites. *J. Compos.* **2014**, *2014*, 838975. [[CrossRef](#)]
18. Shauloff, N.; Prishkolnik, N.; Singh, S.; Manikandan, R.; Ben Nun, U.; Jelinek, R. Carbon Dot / Thermo-Responsive Polymer Capacitive Wavelength-Specific Photodetector. *Carbon* **2023**, *213*, 118211. [[CrossRef](#)]
19. Mondal, A.; Reddy, Y.A.K. Influence of Oxygen Partial Pressure on the Performance of MoO₃-Based Ultraviolet Photodetectors. *Surf. Interfaces* **2023**, *41*, 103179. [[CrossRef](#)]
20. Yuan, M.; Jiang, B.; Zeng, L.; Zeng, C.; Lin, R.; Xin, W.; Yan, G.; Hong, R. Nanosecond-Response Cu(In,Ga)Se₂ Self-Powered Photodetectors Enhanced by the Back Contact Modification. *Appl. Surf. Sci.* **2023**, *637*, 157867. [[CrossRef](#)]
21. Zeng, Z.; Wang, D.; Fang, X.; Zhao, C.; Zhang, B.; Liu, D.; Chen, T.; Pan, J.; Liu, S.; Liu, G.; et al. Self-Powered Broadband Photodetector Based on Bi₂Se₃/GaN Pn Mixed-Dimensional Heterojunction with Boosted Responsivity. *Mater. Today Nano* **2023**, *23*, 100372. [[CrossRef](#)]
22. Shi, K.; Luo, M.; Ying, J.; Zhen, S.; Xing, Z.; Chen, R. Extraction of Lithium from Single-Crystalline Lithium Manganese Oxide Nanotubes Using Ammonium Peroxodisulfate. *iScience* **2020**, *23*, 101768. [[CrossRef](#)] [[PubMed](#)]
23. Wang, T.; Wang, Y.; Zhu, L.; Lv, L.; Hu, Y.; Deng, Z.; Cui, Q.; Lou, Z.; Hou, Y.; Teng, F. High Sensitivity and Fast Response Sol-Gel ZnO Electrode Buffer Layer Based Organic Photodetectors with Large Linear Dynamic Range at Low Operating Voltage. *Org. Electron.* **2018**, *56*, 51–58. [[CrossRef](#)]
24. Wang, Y.; Zhu, L.; Wang, T.; Hu, Y.; Deng, Z.; Cui, Q.; Lou, Z.; Hou, Y.; Teng, F. Fast and Sensitive Polymer Photodetectors with Extra High External Quantum Efficiency and Large Linear Dynamic Range at Low Working Voltage Bias. *Org. Electron.* **2018**, *62*, 448–453. [[CrossRef](#)]
25. Hou, P.; Wang, C.; Chen, Y.; Zhong, Q.; Zhang, Y.; Guo, H.; Zhong, X.; Wang, J.; Ouyang, X. Ionization Effect and Displacement Effect Induced Photoresponsivity Degradation on α-In₂Se₃ Based Transistors for Photodetectors. *Radiat. Phys. Chem.* **2020**, *174*, 108969. [[CrossRef](#)]
26. Al-Jumaili, B.E. Fabrication and Photoresponsive Characteristics of ZnO Film for Ultraviolet ZnO/Porous Si Photodetector: The Effect of Post-Processing Treatment. *Opt. Mater.* **2022**, *133*, 112897. [[CrossRef](#)]
27. Hong, Q.; Cao, Y.; Xu, J.; Lu, H.; He, J.; Sun, J.L. Self-Powered Ultrafast Broadband Photodetector Based on p-n Heterojunctions of CuO/Si Nanowire Array. *ACS Appl. Mater. Interfaces* **2014**, *6*, 20887–20894. [[CrossRef](#)]
28. Kalra, A.; Vura, S.; Rathkanthiwar, S.; Muralidharan, R.; Raghavan, S.; Nath, D.N. Demonstration of High-Responsivity Epitaxial β-Ga₂O₃/GaN Metal-Heterojunction-Metal Broadband UV-A/UV-C Detector. *Appl. Phys. Express* **2018**, *11*, 064101. [[CrossRef](#)]

29. Zheng, L.; Yu, P.; Hu, K.; Teng, F.; Chen, H.; Fang, X. Scalable-Production, Self-Powered TiO₂ Nanowell-Organic Hybrid UV Photodetectors with Tunable Performances. *ACS Appl. Mater. Interfaces* **2016**, *8*, 33924–33932. [[CrossRef](#)]
30. Lan, T.; Fallatah, A.; Suiter, E.; Padalkar, S. Size Controlled Copper (I) Oxide Nanoparticles Influence Sensitivity of Glucose Biosensor. *Sensors* **2017**, *17*, 1944. [[CrossRef](#)]
31. Tan, W.C.; Shih, W.H.; Chen, Y.F. A Highly Sensitive Graphene-Organic Hybrid Photodetector with a Piezoelectric Substrate. *Adv. Funct. Mater.* **2014**, *24*, 6818–6825. [[CrossRef](#)]
32. Bai, Z.; Zhang, Y. Self-Powered UV-Visible Photodetectors Based on ZnO/Cu₂O Nanowire/Electrolyte Heterojunctions. *J. Alloys Compd.* **2016**, *675*, 325–330. [[CrossRef](#)]
33. Costas, A.; Florica, C.; Preda, N.; Apostol, N.; Kuncser, A.; Nitescu, A.; Enculescu, I. Radial Heterojunction Based on Single ZnO-Cu_xO Core-Shell Nanowire for Photodetector Applications. *Sci. Rep.* **2019**, *9*, 5553. [[CrossRef](#)]
34. Chen, Z.; Ci, H.; Tan, Z.; Dou, Z.; Chen, X.-D.; Liu, B.; Liu, R.; Lin, L.; Cui, L.; Gao, P.; et al. Growth of 12-Inch Uniform Monolayer Graphene Film on Molten Glass and Its Application in PbI₂-Based Photodetector. *Nano Res.* **2019**, *12*, 1888–1893. [[CrossRef](#)]
35. Ismail, R.A.; Mousa, A.M.; Shaker, S.S. Visible-Enhanced Silver-Doped PbI₂ Nanostructure/Si Heterojunction Photodetector: Effect of Doping Concentration on Photodetector Parameters. *Opt. Quantum Electron.* **2019**, *51*, 362. [[CrossRef](#)]
36. Wang, S.B.; Hsiao, C.H.; Chang, S.J.; Lam, K.T.; Wen, K.H.; Hung, S.C.; Young, S.J.; Huang, B.R. A CuO Nanowire Infrared Photodetector. *Sens. Actuators A Phys.* **2011**, *171*, 207–211. [[CrossRef](#)]
37. Naldoni, A.; Guler, U.; Wang, Z.; Marelli, M.; Malara, F.; Meng, X.; Besteiro, L.V.; Govorov, A.O.; Kildishev, A.V.; Boltasseva, A.; et al. Broadband Hot-Electron Collection for Solar Water Splitting with Plasmonic Titanium Nitride. *Adv. Opt. Mater.* **2017**, *5*, 1601031. [[CrossRef](#)]
38. Liu, K.; Sakurai, M.; Liao, M.; Aono, M. Giant Improvement of the Performance of ZnO Nanowire Photodetectors by Au Nanoparticles. *J. Phys. Chem. C* **2010**, *114*, 19835–19839. [[CrossRef](#)]
39. Zheng, L.; Hu, K.; Teng, F.; Fang, X. Novel UV-Visible Photodetector in Photovoltaic Mode with Fast Response and Ultrahigh Photosensitivity Employing Se/TiO₂ Nanotubes Heterojunction. *Small* **2017**, *13*, 1602448. [[CrossRef](#)]

Disclaimer/Publisher's Note: The statements, opinions and data contained in all publications are solely those of the individual author(s) and contributor(s) and not of MDPI and/or the editor(s). MDPI and/or the editor(s) disclaim responsibility for any injury to people or property resulting from any ideas, methods, instructions or products referred to in the content.